Physics of Fluids ARTICLE pubs.aip.org/aip/pof

Internal tsunami waves in a stratified ocean induced by explosive volcano eruption: A parametric source

Cite as: Phys. Fluids **36**, 042110 (2024); doi: 10.1063/5.0206121
Submitted: 29 February 2024 · Accepted: 2 April 2024 ·
Published Online: 18 April 2024

View Online Export Citation CrossMark

Tatiana Talipova,[1,2] Efim Pelinovsky,[1,3] and Ekaterina Didenkulova[1,3,a)]

AFFILIATIONS

[1]A.V. Gaponov-Grekhov Institute of Applied Physics of the Russian Academy of Sciences, 46 Ulyanov Str., 603950 Nizhny Novgorod, Russia
[2]Il'ichev Pacific Oceanological Institute Far Eastern Branch, Russian Academy of Sciences, 43 Baltiyskaya Street, Vladivostok 690041, Russia
[3]Faculty of Informatics, Mathematics and Computer Science, HSE University, 25/12 Bolshaya Pecherskaya Street, 603155 Nizhny Novgorod, Russia

[a)]**Author to whom correspondence should be addressed:** edidenkulova@hse.ru

ABSTRACT

This article discusses the problem of generating internal waves during explosive eruptions of underwater volcanoes. The importance and novelty of such studies are associated with the emerging data on the observation of internal waves during a volcanic eruption in the Tonga Archipelago in 2022 reported in Zhang and Li ["Oceanic internal waves generated by the Tongan volcano eruption," Acta Oceanol. Sin. **41** (8), 1–4 (2022)]. Using Le Méhaute's parametric model originally suggested to calculate surface waves, internal waves in the ocean with a constant buoyancy frequency are calculated. Internal waves are trains of different modes, the parameters of which were found for different ratios between the radius of the equivalent source and the depth of the basin. Even at relatively small distances from the source (tens of km), wave amplitudes changeover time periods consisting of several days, which confirms the possibility of delineating the tsunami source by internal waves.

I. INTRODUCTION

Explosive eruptions of volcanoes, underwater or located near the shore, often generate tsunami waves. It is enough to mention the most famous historical event of 1883, i.e., the eruption of the Krakatoa volcano in Indonesia, when tsunami waves reached a height of almost 40 m and killed about 36 000 people in the Sunda Strait (see, for example, Ref. 2). After leaving the strait, the waves spread throughout the Indian Ocean; sea level fluctuations had also been noted in the Atlantic and Pacific oceans.[3,4] Since then, the number of registered tsunami waves of volcanic origin in seas and lakes has increased significantly. Let us note, in particular, the eruption of an underwater volcano in Lake Karymskoye (Kamchatka, Russia) in January 1996, which produced a tsunami up to 30 m high (see, for example, Ref. 5). The latest event, the volcanic eruption in the Tonga archipelago on January 15, 2022, which aroused great interest in the world, was accompanied by tsunami waves and sea level disturbances around the world (along with atmospheric and ionospheric disturbances); see, for example, Refs. 6 and 7.

The physics of a volcanic eruption is quite complex[8] and is dictated by the hydromechanics that control the rise of magma. Ascent is influenced not only by the nucleation and growth of gas bubbles but also by the rheology of the magma and its fragmentation. Depending on the balance of different forces, a volcanic eruption can occur slowly or quickly in an explosive manner. Tsunami waves occur during explosive volcanic eruptions, and here several mechanisms can be distinguished: earthquakes initiated by a volcanic eruption; pyroclastic flows from the slopes of the volcano; caldera collapse; underwater explosions.[9] The last two mechanisms are, to some extent, identical and manifest themselves in the eruption of a finite mass of matter and the appearance of a large gas bubble, which leads to the curvature of the water surface and gives rise to the generation of tsunami waves. In this case, due to the compressibility of seawater, strong shock waves arise, partially reflected from the water surface, also deforming it.[10] Due to the large nonlinearity and the presence of several interacting processes, there is no rigorous theoretical model for the generation of tsunami waves during the eruption of underwater volcanoes of the type developed for tsunamis of seismic origin. The most popular is Le Mehaute's parametric model (see the latest version in Ref. 11, which proposes a model of the source of blast waves, which is determined by the explosion energy. This model is widely used for cosmogenic tsunamis,[12–14] and it was also used to interpret data from the volcanic tsunami near Japan (Myojinsho Volcano) in 1952[15] and in 1996 in Lake Karymskoye.[5]

Along with this, the theory also considers the classical formulation of the linear problem of wave generation, which usually occurs at a point source of mass located at depth as a model of wave generation by an explosive volcanic eruption.[16–18] Within the framework of such a model, the determining parameters are the mass of erupted material, the height of the underwater volcano, and the time of the eruption, which was not taken into account in Le Mehaute's parametric model. The presence of several parameters makes it possible to better approximate the results of calculations to observational data, as demonstrated by the example of the Myojinsho Volcano eruption in 1952.[18] This model should also be taken into account when describing the wave field far away from the source when it becomes linear.

In all the works listed above, the stratification of sea waters was neglected. Meanwhile, the analysis of satellite images obtained by the synthetic aperture radar (SAR) of the European Space Agency's Sentinel-1 showed the appearance of internal waves near the volcano after its eruption.[1] The observed internal waves are not as dangerous as tsunami surface waves; they propagate very slowly (no more than 1–3 m/s), and, therefore, remain near the source for a long time, outlining it. As a result, additional information about the tsunami source can be obtained.

The mechanisms for generating internal waves during the eruption of underwater volcanoes can be different. The first of them is similar to the generation of tsunami surface waves during an explosion and is associated with the curvature of the interface between layers of different densities (isopycnals). This mechanism is included in tsunami calculations in the recent work,[19] although without emphasizing the characteristics of the internal waves that are generated. The second mechanism may be due to hot gravitational pyroclastic flows from the volcanic slope, playing the role of a piston in the curvature of isopycnals. It is this mechanism (albeit without confirmation) that has been proposed to interpret satellite observations of internal waves during a volcanic eruption in the Tonga archipelago.[1] A third mechanism for the generation of internal waves during the transformation of long surface tsunami waves on the continental slope is also possible. It is similar to the generation of internal waves on the slope during the transformation of the barotropic tide[20] by an explosive volcanic eruption within the first mechanism, when caldera collapse results in the curvature of the interface between layers of different densities.

Our goal is to obtain estimates of the internal waves that can occur during an underwater volcanic eruption. For simplicity, we assume that stratification is determined by a constant buoyancy frequency. As the tsunami source, we choose the parametric Le Mehaute's model; it is briefly described in Sec. II. Derived formulas within the framework of the linear theory of cylindrical waves are given in Sec. III. The results of calculations for shallow and deep seas are given in Sec. IV. The results obtained are summarized in the Conclusion.

II. PARAMETRIC MODEL OF A TSUNAMI SOURCE

Based on data from numerous experiments with explosions in water, in the works of Le Mehaute and co-workers (see the review[21] and book[11]), a parametric tsunami source was formulated in the form of a parabolic cavern (Fig. 1):

$$\eta_e(r) = H_e \begin{cases} 2\left(\dfrac{r}{R}\right)^2 - 1, & r < R, \\ 0, & r > R, \end{cases} \tag{1}$$

where the typical height H_e and the cavern radius R depend on the characteristics of the explosion, primarily on the energy of the explosion. The dependences of the displacement amplitude and source radius on the eruption energy can be approximated by formulas (2). The regression formulas have the following form (Fig. 2):

$$H_e \approx 0.02E^{0.24}, \qquad R \approx 0.04E^{0.3}. \tag{2}$$

Here, the explosion energy E is measured in joules, and the height and radius are measured in meters. In general, the numerical coefficients in (2) also depend on the depth of the basin and can change almost twice; we chose average values to simplify subsequent calculations. It should be noted that in various reports about the eruption characteristics, the ejected substance volume (V) often appears in lieu of the explosion energy. The following relationship between these characteristics is proposed in Ref. 22:

$$E \approx 4 \cdot 10^6 V^{1.1}. \tag{3}$$

Thus, the parameters of the source can also be expressed through the volume of the ejected substance.

Although these empirical formulas were derived for underwater explosions, they have already been used to interpret data from volcanic tsunamis in Japan (Myojinsho Volcano) in 1952 (Ref. 15) and in Kamchatka's Lake Karymskoye in 1996 (Ref. 5) and showed a good agreement with the observed data.

To our knowledge, the theoretical and experimental study of the internal wave generation during the volcano eruption has not been done early. Therefore, the applicability of the parametric Le Mehaute's source to internal waves requires experimental verification. However, the very good suitability of such a source for surface waves gives us confidence that the same model will work for internal waves as well.

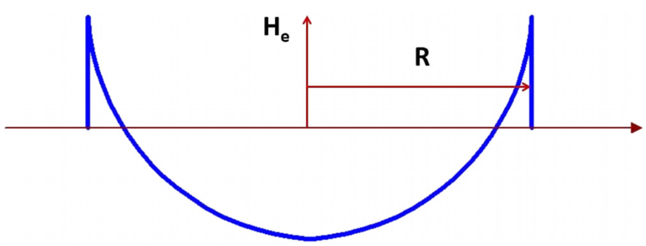

FIG. 1. Initial cavern of the parametric source.

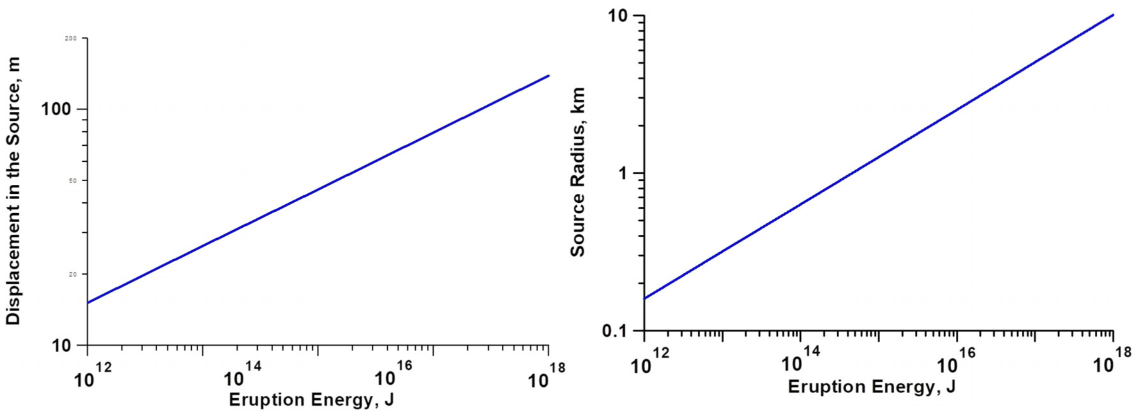

FIG. 2. The relationships between the characteristics of the parametric source and the energy of the eruption.

III. WAVE FIELD ARISING FROM THE ERUPTION OF AN UNDERWATER VOLCANO

A parametric source, coupled with a zero initial condition on the displacement velocity of water particles, was used to describe the far wave field within the framework of the linear theory of water waves. We use it below to describe waves in a stratified sea. It is natural to assume that the waves generated during the eruption of underwater volcanoes are quite long and cover the entire thickness of the ocean. In this case, the wave field in a stratified ocean can be represented by a set of eigenmodes,

$$\eta(z,x,y,t) = \sum_{n=1}^{\infty}\int\int A_n(k_x,k_y)\Phi_n(z,k_x,k_y)\exp\left[i(\omega t - k_x x - k_y y)\right]dk_x dk_y, \tag{4}$$

where A_n—spectral amplitudes, Φ_n—modal function, and ω—wave frequency determined from the boundary value problem (Sturm–Liouville problem),

$$\frac{d^2\Phi_n}{dz^2} + k^2\frac{N^2(z)-\omega_n^2}{\omega_n^2}\Phi_n = 0, \tag{5}$$

with zero boundary conditions on the bottom and free surface of the basin (here, the Boussinesq approximation standard for oceanic conditions and the solid lid approximation on the surface are used).[23] Here, $N(z)$ is the buoyancy frequency (Väisälä–Brent frequency), determined through the seawater density gradient $\rho(z)$,

$$N(z) = \sqrt{\frac{g}{\rho(z)}\frac{d\rho(z)}{dz}}, \tag{6}$$

where g—acceleration due to gravity and the z axis is directed deep into the liquid.

In the case of a cylindrical problem (it is characteristic of waves during the eruption of underwater volcanoes), formula (4) is transformed into

$$\eta(z,r,t) = \sum_{n=1}^{\infty}\int_0^{\infty} kA_n(k)\Phi_n(z,k)J_0(kr)\cos(\omega_n t)dk, \tag{7}$$

where J_0—zero order Bessel function. The spectral amplitude is determined through the Hankel (Bessel–Fourier) transform of the initial disturbance

$$A_n(k) = \frac{1}{\int_0^h \Phi_n^2(k,z)dz}\int_0^{\infty} rJ_0(kr)dr\int_0^h \eta(z,r,0)\Phi_n(z,k)dz, \tag{8}$$

where h—basin depth.

Formulas (7) and (8) make it possible to calculate the linear wave field from any initial displacements in the source and arbitrary stratification of the ocean. It can be assumed that during an explosive eruption of an underwater volcano, all layers in the ocean shift almost simultaneously to the same height. In this case, the function $\eta(z, r, 0)$ can be considered independent of the vertical coordinate z, and replaced by $\eta_e(r)$ according to Eq. (1). As a result, we obtain a formula for calculating spectral amplitudes,

$$A_n(k) = \frac{\int_0^h \Phi_n(z,k)dz}{\int_0^h \Phi_n^2(k,z)dz}\int_0^{\infty} r\eta_e(r)J_0(kr)dr. \tag{9}$$

IV. WAVES IN A SEA WITH A CONSTANT BUOYANCY FREQUENCY (RESULTS OF THE COMPUTATIONS)

We perform specific calculations for an ocean with a constant Väisälä–Brent frequency $N = const$. In this case, boundary value problem (5) for internal waves is easily solved analytically,

$$\Phi_n(z) = \sin(n\pi z/h), \quad \omega_n(k) = \sqrt{\frac{N^2k^2}{k^2 + (n\pi/h)^2}}. \tag{10}$$

Dispersion curves $\omega(k)$ and group velocity $c(k) = d\omega/dk$ are presented in Fig. 3 in dimensionless variables (ω/N, kh) for the three lowest modes.

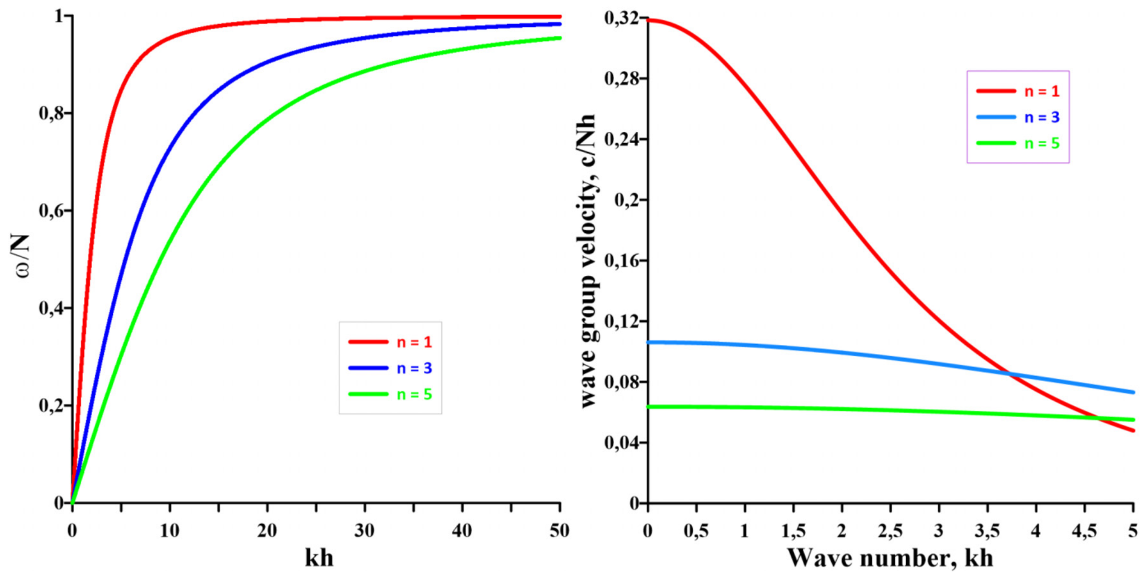

FIG. 3. Dispersion curves $\omega(k)$ and group velocity $c(k)$ for internal waves in a medium with constant buoyancy frequency.

It is important that the structure of modes of internal waves does not depend on the wave number, and all integrals in (7) and (9) are simplified. Thus, the spectral amplitudes are nonzero only for odd modes ($n = 2m + 1$),

$$A_m(k) = \frac{4}{\pi(2m+1)}\int_0^\infty r\eta_e(r)J_0(kr)dr, \quad m = 0, 1, 2, \ldots. \tag{11}$$

The integral here is exactly the same as for surface waves.[11,21] Therefore, we instantly provide the final answer

$$A_m(k) = \frac{4H_eR^2}{\pi(2m+1)}F(kR), \quad m = 0, 1, 2, \ldots, \tag{12}$$

where the dimensionless spectral function is (J_3 is the Bessel function of the third order)

$$F(\theta) = -\frac{J_3(\theta)}{\theta}. \tag{13}$$

The graph of this function is shown in Fig. 4. As we can see, the spectrum contains spatial frequencies determined by the effective radius of the source kR in the range 0–10; shorter waves have small amplitudes. The absence of a zero component in the spectrum is also explainable due to the zero net volume displacement, which is easily verified by calculation using Eq. (1).

The wave field itself is the sum of odd partial modes derived from (7) and (12),

$$\eta(z, r, t) = \frac{4H_e}{\pi}\sum_{m=0}^{\infty}\Psi_m(r, t)\frac{\sin[(2m+1)\pi z/h]}{2m+1}, \tag{14}$$

where

$$\Psi_m(r, t) = R^2\int_0^\infty kF(kR)J_0(kr)\cos(\omega_m t)dk. \tag{15}$$

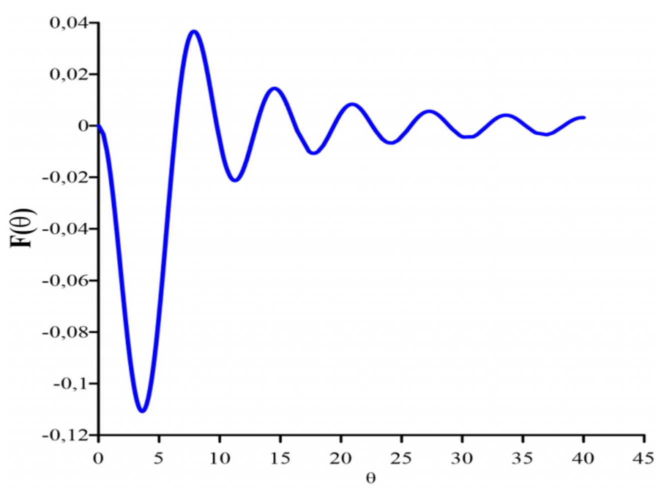

FIG. 4. Dimensionless spectral amplitude of internal waves in a medium with a constant buoyancy frequency.

It is convenient to re-scale the distance by the radius of the source ($x = r/R$), time—by the Väisälä–Brent frequency ($\tau = Nt$), wave number by the source radius ($\theta = kR$), then the function Ψ simplifies as much as possible and depends on only one parameter Π—the ratio of the source radius to the basin depth,

$$\Psi_m(x, \tau; \Pi_m) = \int_0^\infty \theta F(\theta)J_0(x\theta)\cos(\Omega_m\tau)d\theta, \tag{16}$$

$$\Omega_m = \sqrt{\frac{\theta^2}{\theta^2 + \Pi_m^2}}, \quad \Pi_m = \frac{(2m+1)\pi R}{h}. \tag{17}$$

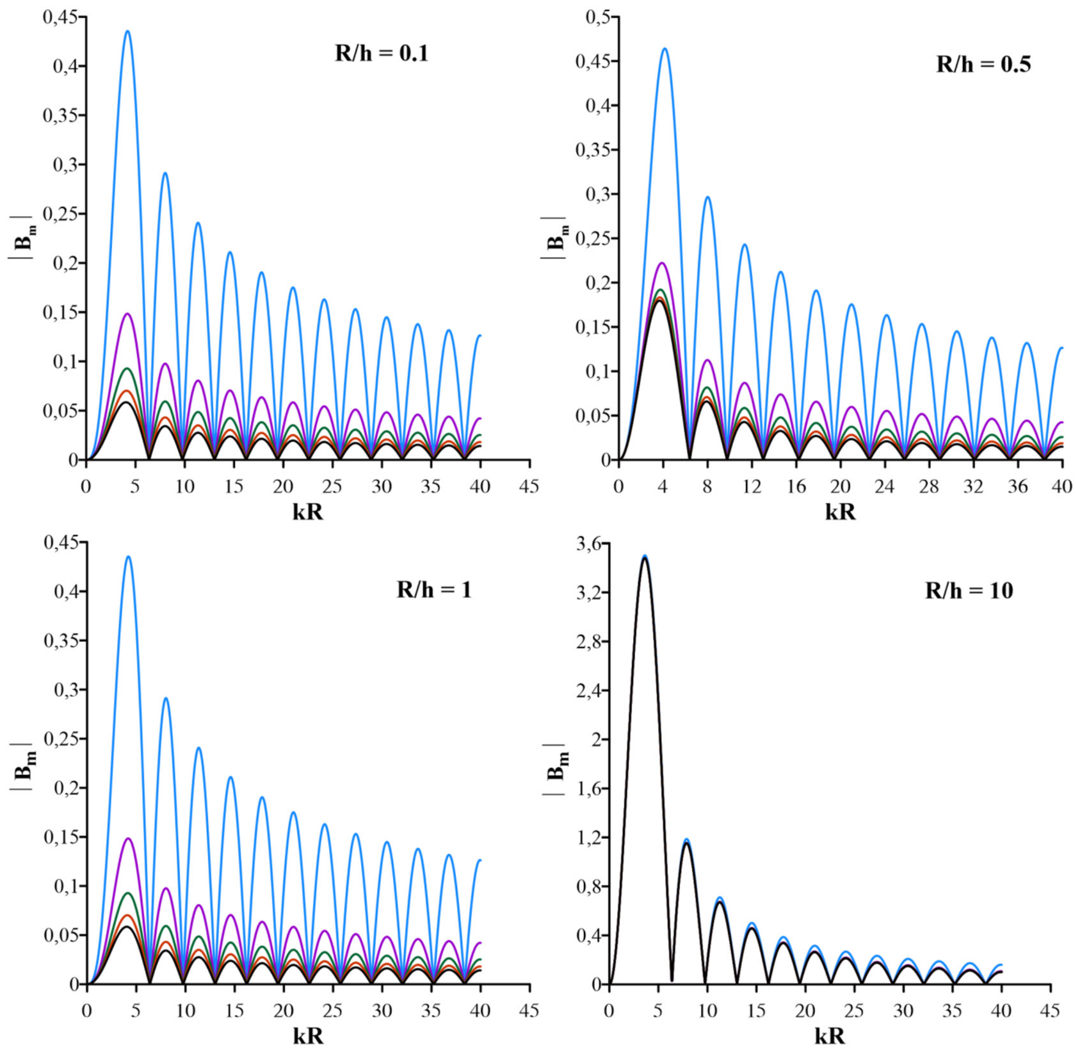

FIG. 5. Spatial spectral amplitudes of wave trains. The upper curve in all figures corresponds to the first mode $n = 1$ ($m = 0$); as the number increases, the curves decrease in amplitude (curves with $m = 0$–4 are shown).

Using formulas (14) and (16), one can calculate the wave field at any time and at any distance from the source. However, as has been repeatedly stated above, a parametric source was introduced in order to exclude the source zone with complex processes in it and to be able to calculate the far field within the framework of the linear theory. At a large distance ($x = r/R \gg 1$), we use the asymptotic formula for the Bessel function,

$$J_0(x\theta) \approx \sqrt{\frac{2}{\pi x\theta}}\cos\left(x\theta - \frac{\pi}{4}\right), \tag{18}$$

and calculate the integral (16) using the stationary phase method (see, for example, Wong, 2001),

$$\Psi_m(x,\tau) = \frac{1}{2\pi x}\sqrt{\frac{\theta c_m(\theta)}{|dc_m/d\theta|}}F(\theta)\cos\left[\theta x - \Omega_m(\theta)\tau \pm \frac{\pi}{4}\right], \tag{19}$$

where the dimensionless wave number θ can be found from the equation for group velocity

$$c_n(\theta) = \frac{d\Omega_n(\theta)}{d\theta} \approx \frac{x}{\tau} \tag{20}$$

and depends on time at a fixed distance from the source. Calculating the group velocity from formula (17), we obtain the final expression for the function Ψ,

$$\Psi_m(x,\tau) = \frac{1}{2\pi x}\sqrt{\frac{\theta^2 + \Pi_m^2}{3}}F(\theta)\cos\left[\theta x - \Omega_m(\theta)\tau \pm \frac{\pi}{4}\right]. \tag{21}$$

As a result, we obtain the final formula for the far-field of internal waves,

$$\eta(z,x,\tau) = \frac{2H_e}{\sqrt{3\pi^2 x}}\sum_{m=0}^{\infty} B_m(\theta)\cos\left[\theta x - \Omega_m(\theta)\tau \pm \frac{\pi}{4}\right]\sin[(2m+1)\pi z/h], \tag{22}$$

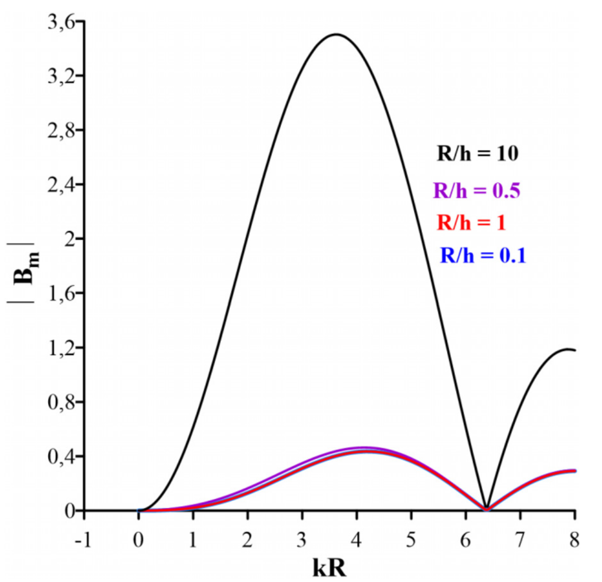

FIG. 6. Spectral composition of the leading train of internal waves of the lowest mode depending on the ratio of the source radius to the depth of the basin.

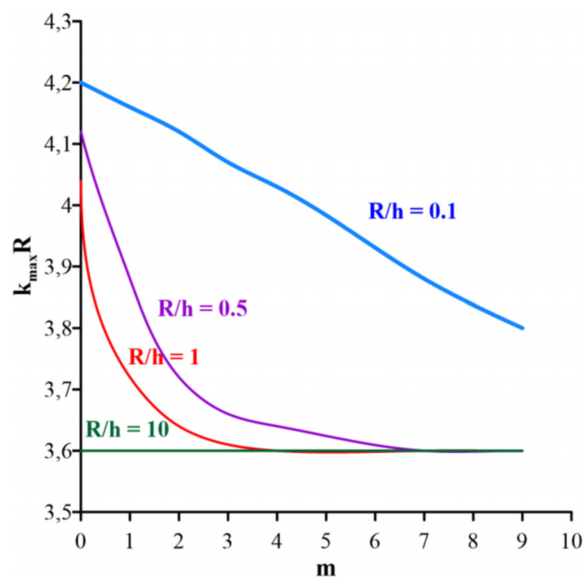

FIG. 8. Dependence of the wave number of the wave of maximum amplitude in the leading train on *m*.

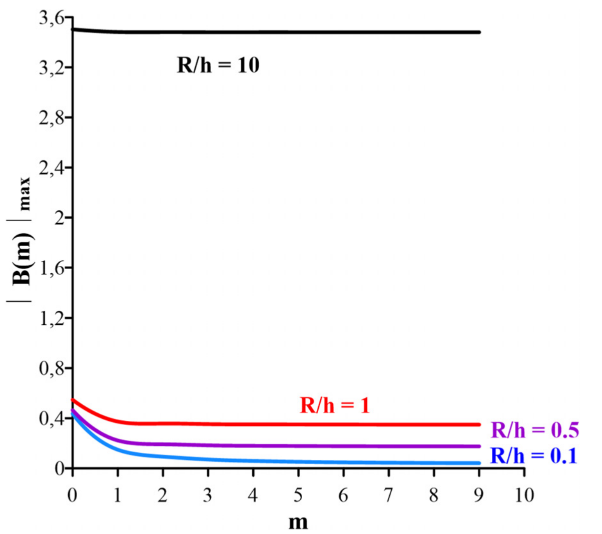

FIG. 7. Dependence of the maximum amplitude of the leading train at different *R/h* on *m*.

$$B_m(\theta) = \frac{F(\theta)\sqrt{\Pi_m^2 + \theta^2}}{2m+1}, \tag{23}$$

$$\theta = \sqrt{\left(\frac{\Pi_m^2 \tau}{x}\right)^{2/3} - \Pi_m^2}. \tag{24}$$

It should be said that the stationary phase method is not applicable in the vicinity of $\theta \sim 0$, which is already evident from the asymptotic formula (18). However, in contrast to the similar problem of excitation of tsunami waves by vertical movements of the bottom, where this problem is emphasized,[24] our spectral amplitude B_m is small in the vicinity of small wavenumbers, so this region of the spectrum does not affect the characteristics of internal tsunami waves.

Thus, the wave field is represented by the sum of modes (recall that the mode number $n = 2m+1$), each of which propagates in the form of a frequency-modulated pulse with its own group velocity, decreasing in space in inverse proportion to the distance. The wavenumber spectrum of a frequency-modulated pulse is characterized by the amplitude $|B_m(\theta)|$ shown in Fig. 5 for different values of the ratio of the radius of the source to the depth of the basin *R/h*. Let us immediately note that for all modes and magnitudes of the ratio *R/h*, the maximum amplitudes are relatively long waves with values $kR < 6.4$ (first zero of the function J_3), so the most dangerous are the first trains of each mode. The second and subsequent trains are especially small when the eruption occurs in a shallow sea ($R > h$), and then the amplitude of subsequent trains decreases by more than half (Fig. 5 at the bottom). The speed of the "long" head train of the first mode is the highest, so it arrives first at the observation point. Then, waves of different modes with different frequencies arrive, interfering with each other.

Let us study in more detail the characteristics of the leading train of internal waves. The spectral composition of the lowest mode head train is shown in Fig. 6. Regardless of the depth of the basin, the width of the spectrum of the leading train is the same and equal to $kR = 6.4$. Spectral amplitudes are sensitive to the R/h ratio and are maximum in shallow seas.

The maximum amplitude of the train is defined as the extremum of formula (23); it is shown in Fig. 7 as a function of the number *m*, which determines the mode number.

Waves generated in shallow sea ($R \gg h$) practically do not depend on the mode number, which is obvious from the asymptotics of Eq. (23),

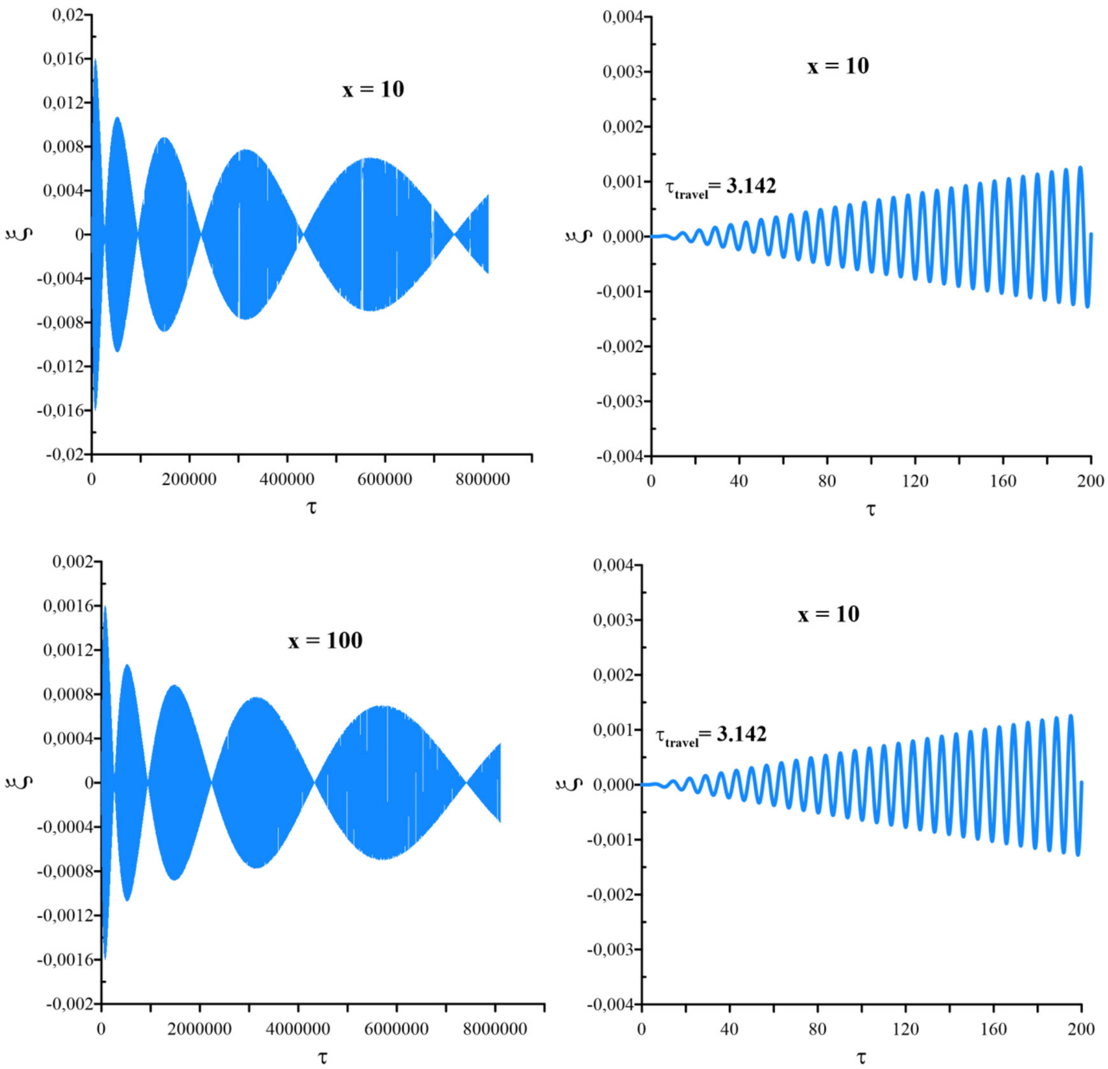

FIG. 9. Mareogram of the lowest mode ($m = 0$) at different distances from the source on the horizon $z = h/2$ in the case of deep sea ($R/h = 0.1$) in dimensionless variables.

$$B_m(\theta; R/h \to \infty) \approx \pi F(\theta)\frac{R}{h}. \tag{25}$$

Thus, in a shallow sea, almost identical (in amplitude) trains of different modes with a time delay and different characteristic frequencies will arrive at the observation point. In the deep sea, the amplitude of the trains decreases with increasing mode number and here the lowest mode prevails.

The wave of maximum amplitude in the leading train of each mode has a fixed wave number $Rk_{\max}$, shown in Fig. 8 depending on m, and, consequently, a fixed wavelength proportional to the radius of the parametric source. In shallow seas $Rk_{\max} = 3.6$, and this value is constant for all modes. For higher modes, the maximum occurs at shorter wavelengths. The wave of maximum amplitude in the leading train of each mode moves at a constant speed,

$$c_m = \frac{\Pi_m^2}{\left[\Pi_m^2 + (kR)_{\max}^2\right]^{3/2}} = \frac{x}{\tau}, \quad \Pi_m = \frac{(2m+1)\pi R}{h}. \tag{26}$$

In the case of shallow seas, as one would expect, the wave of a maximum amplitude moves at almost the maximum speed of long waves,

$$c_m \approx \frac{1}{\Pi_m}\left[1 - \frac{3(Rk_{\max})^2}{2\Pi_m^2}\right], \tag{27}$$

or in a dimensional form,

$$(C_{gr})_m \approx \frac{Nh}{(2m+1)\pi}\left[1 - \frac{3h^2k_{\max}^2}{2(2m+1)^2\pi^2}\right]. \tag{28}$$

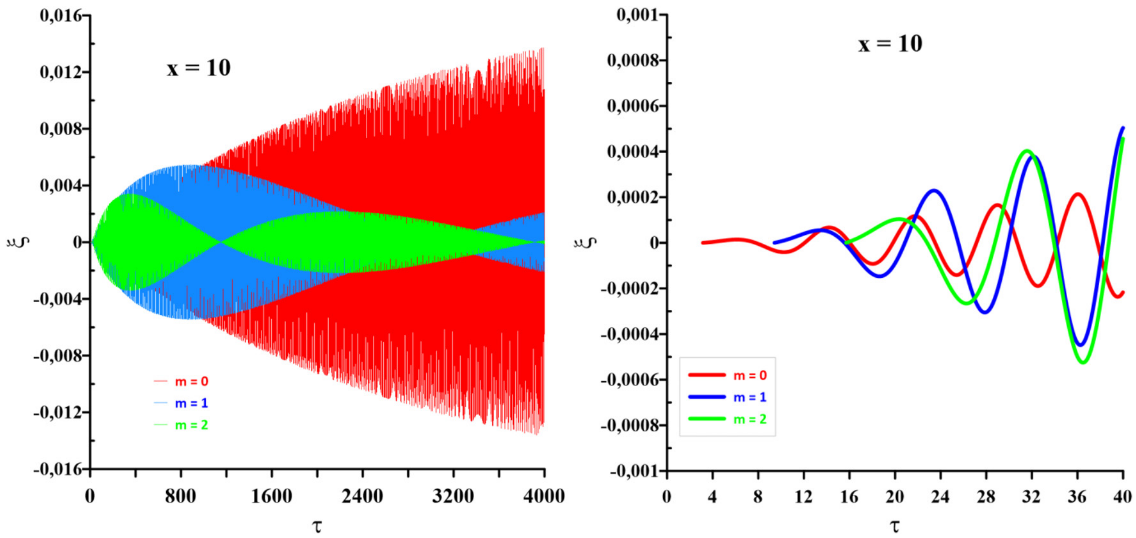

FIG. 10. Mareograms of waves of three modes ($m = 0$—red line, $m = 1$—blue line, и $m = 2$—green line) at point $x = 10$ ($R/h = 0.1$). On the right the initial stage of mariograms is given.

Here, we present a mariogram of the lowest mode ($m = 0$) at different distances from the source on the horizon $z = h/2$ in the case of a deep sea ($R/h = 0.1$), constructed according to Eq. (22) in dimensionless variables: $\xi = \eta/H_e$, $\tau = Nt$, $x = r/R$ (Fig. 9). On the left is a "complete" mareogram containing several trains of internal waves. Its initial part is on the right, clearly showing the time of arrival of the head wave (t_{start}) and the linear character of the increase in amplitude along the train.

In essence, mareograms of internal waves of other modes are qualitatively similar to those shown in Fig. 9. They are shown in Fig. 10. Naturally, the arrival time of each mode is different and is actually determined by the maximum group velocity; see formulas (27) or (28). The difference in the velocities of the first and third modes ($m = 0$ and $m = 1$) reaches 3; the time of arrival at the point $x = 10$ is 3.14 and 9.42, respectively. The fifth mode ($m = 2$) arrives at the observation point at the moment 15.7, i.e., five times longer than the first, which is clearly visible in Fig. 10(b). However, the strongest visible effect is the significantly different time scales of carrier waves and envelope waves. As already mentioned, the spatial scales of wave groups are the same and are determined by the zeros of the Bessel function, but the time scales change significantly due to the strong difference in group velocities. This can already be seen from Eq. (10) and Fig. 3—the group velocity of the highest mode may be higher than the velocity of the lowest mode.

Thus, in Fig. 10, plotted for $x = 10$, the leading train of the third mode (green line) ends first, the leading train of the second mode (blue line) is more extended, while the leading train of the first mode (red line) has not reached its maximum yet. Dimensionless timescale (4000) in Fig. 10 corresponds to approximately 700 Väisälä–Brent periods. In the case of, for example, a Väisälä–Brent period of 5 min, we get approximately 60 h. Thus, internal waves, even at short distances from the source, exist for quite a long time, which is important for delineating the tsunami source.

V. CONCLUSION

The first report on the observation of internal waves after a volcanic eruption in the Tonga archipelago on January 15, 2022 served as the starting point for our theoretical analysis of internal waves generated during underwater volcanic eruptions. The Le Mehaute's parabolic cavern, which is actively used in calculating surface tsunami waves during explosions in water, eruptions of underwater volcanoes, and meteorite falls into water, was adopted as the source of tsunami waves. It is assumed that the isopycnals above the underwater volcano are curved in the same way as the water surface. Within the framework of linear theory, the wave field in the ocean with a constant buoyancy frequency is calculated. Calculations have shown the generation of a multimode field of internal waves propagating in the form of trains. The most intense are the leading trains of each mode. The arrival time of waves of different modes and the wave of the lowest mode always arrives first. The characteristic frequencies of individual waves in trains increase with the mode number. Due to the entanglement of the group velocity curves of different modes, there is a complex interference of groups of waves of different modes. It should be noted that over time, at the observation point, it is the trains of higher modes that may turn out to be more intense than the leading train of the lowest mode. The duration of trains of internal waves reaches thousands of Väisälä–Brent periods, so that even at relatively small distances from the source of tens of kilometers, internal waves remain noticeable for several trains. This provides grounds for delineating the source of an underwater eruption using contact or remote measurements of internal waves.

ACKNOWLEDGMENTS

The research is carried out with the support of the Russian Science Foundation Grant No. 24-27-00110.

AUTHOR DECLARATIONS

Conflict of Interest

The authors have no conflicts to disclose.

Author Contributions

Tatiana Talipova: Conceptualization (equal); Investigation (equal); Methodology (equal); Visualization (equal); Writing – original draft (equal). **Efim Pelinovsky:** Conceptualization (equal); Investigation (equal); Methodology (equal); Writing – original draft (equal); Writing – review & editing (equal). **Ekaterina Didenkulova:** Conceptualization (equal); Investigation (equal); Methodology (equal); Writing – review & editing (equal).

DATA AVAILABILITY

Data sharing is not applicable to this article as no new data were created or analyzed in this study.

REFERENCES

[1] X. Zhang and X. Li, "Oceanic internal waves generated by the Tongan volcano eruption," Acta Oceanol. Sin. **41**(8), 1–4 (2022).

[2] T. Simkin and R. S. Fiske, *Krakatau 1883 - The Volcanic Eruption and Its Effects* (Smithsonian Institution Press, 1983).

[3] G. J. Symons, "The eruption of Krakatoa and subsequent phenomena," Report of the Krakatoa committee of the Royal Society (Trubner & Co, 1888).

[4] E. Pelinovsky, B. H. Choi, A. Stromkov, I. Didenkulova, and H. S. Kim, "Analysis of tide-gauge records of the 1883 Krakatau tsunami," in *Tsunamis: Case Studies and Recent Developments, Advances in Natural and Technological Hazards Research* (Springer, 2005), pp. 57–77.

[5] T. Torsvik, R. Paris, I. Didenkulova, E. Pelinovsky, A. Belousov, and M. Belousova, "Numerical simulation of tsunami event during the 1996 volcanic eruption in Karymskoe lake, Kamchatka, Russia," Nat. Hazards Earth Syst. Sci. **10**, 2359–2369 (2010).

[6] J. P. Terry, J. Goff, N. Winspear, V. P. Bongolan, and S. Fisher, "Tonga volcanic eruption and tsunami, January 2022: Globally the most significant opportunity to observe an explosive and tsunamigenic submarine eruption since AD 1883 Krakatau," Geosci. Lett. **9**, 24 (2022).

[7] T. Kubota, T. Saito, and K. Nishida, "Global fast-traveling tsunamis driven by atmospheric Lamb waves on the 2022 Tonga eruption," Science **377**, 91–94 (2022).

[8] H. M. Gonnermann and M. Manga, "The fluid mechanics inside a volcano," Annu. Rev. Fluid Mech. **39**, 321–356 (2007).

[9] R. Paris, "Source mechanisms of volcanic tsunamis," Philos. Trans. R. Soc. A **373**, 20140380 (2015).

[10] M. Holt, "Underwater explisions," Annu. Rev. Fluid Mech. **9**, 187–214 (1977).

[11] B. L. Mehaute and S. Wang, *Water Waves Generated by Underwater Explosion* (World Scientific, 1996).

[12] S. N. Ward and E. Asphaug, "Asteroid impact tsunami: A probabilistic hazard assessment," Icarus **145**, 64–78 (2000).

[13] R. Weiss, K. Wunnemann, and H. Bahlburg, "Numerical modelling of generation, propagation and run-up of tsunamis caused by oceanic impacts: Model strategy and technical solutions," Geophys. J. Int. **167**, 77–88 (2006).

[14] A. Kozelkov and E. Pelinovsky, "Tsunami of meteoric origin," in *Dynamics of Disaster Disasters—Key Concepts, Models, Algorithms, and Insights* (Springer, 2016), pp. 135–157.

[15] N. R. Mirchina and E. N. Pelinovsky, "Estimation of underwater eruption energy based on tsunami wave data," Nat. Hazards **1**(3), 277–283 (1988).

[16] D. G. Duffy, "On the generation of oceanic surface waves by underwater volcanic explosions," J. Volcanol. Geotherm. Res. **50**, 323–344 (1992).

[17] Y. Egorov, "Tsunami wave generation by the eruption of underwater volcano," Nat. Hazards Earth Syst. Sci. **7**, 65–69 (2007).

[18] N. Lipiejko, C. N. Whittaker, E. M. Lane, J. D. L. White, and W. L. Power, "Tsunami generation by underwater volcanic explosions: Application to the 1952 explosions of Myojinsho Volcano," Pure Appl. Geophys. **178**, 4743–4761 (2021).

[19] M. Kanojia, S. Gurusamy, and B. Basu, "Modeling of tsunami generated in stratified oceans by subaquatic volcanic eruptions," Phys. Fluids **35**, 056602 (2023).

[20] V. Vlasenko, N. Stashchuk, and K. Hitter, *Baroclinic Tides* (Cambridge University Press, 2005).

[21] B. Mehaute, "Theory of explosion-generated water waves," Adv. Hydrosci. **7**, 1–79 (1971).

[22] H. Sato and H. Taniguchi, "Relationship between crater size and ejecta volume of recent magmatic and phreato-magmatic eruptions: Implications for energy partitioning," Geophys. Res. Lett. **24**(3), 205–208, https://doi.org/10.1029/96GL04004 (1997).

[23] Y. Z. Miropolsky, *Dynamics of the Internal Gravity Waves in the Ocean* (Springer, 2001).

[24] Y. L. Gazaryan, "On the surface waves in the ocean excited by underwater earthquakes," Akust. Zh. (Acoust. J.) **1**, 203–217 (1955) (in Russian).